Me ab lic e g amming en l e cance cell i al de i e nc genic ignaling bl ckade

H i- en L e,[1] Jennife P d lak,[1] Ke in K lahi,[2] La Cheng,[3] S m a Ra ,[1] De in Ga g,[1] Chang-H i X e,[1] J ha K. Ran ala,[1] Jeff e W. T ne ,[1] Ken L. Th nb g,[2] Ann Ma ine -Ace ed ,[4] Jen-Jane Li ,[4] Ch i he L. Amling,[4] Cha le T ille ,[5] Sha n M. L ie,[6] Kimbe l E. Ande n,[6] Michael J. E an ,[5] Vale ie B. O'D nnell,[7] Daniel K. N m a,[6] J in M. D ake,[3] Anna Ri ,[8] and Ge ge V. Th ma [1,9]

[1]Knight Comprehensive Cancer Institute, Oregon Health and Science University, Portland, Oregon 97239, USA; [2]Knight Cardiovascular Institute, Oregon Health and Science University, Portland, Oregon 97239, USA; [3]Rutgers Cancer Institute of New Jersey, Rutgers, The State University of New Jersey, New Brunswick, New Jersey 08903, USA; [4]Department of Urology, Oregon Health and Science University, Portland, Oregon 97239, USA; [5]Department of Radiology, University of California at San Francisco School of Medicine, San Francisco, California 94107, USA; [6]University of California at Berkeley, Berkeley, California 94720, USA; [7]Systems Immunity Research Institute, Cardiff University, Cardiff CF14 4XN, United Kingdom; [8]Department of Biology, Reed College, Portland, Oregon 97202, USA; [9]Department of Pathology and Laboratory Medicine, Oregon Health and Science University, Portland, Oregon 97239, USA

The e il limi ed kn ledge ab he me ab lic e g amming ind ced b cance he a ie and h hi c n- ib ed he a e ic e i ance. He e e h ha al h gh inhibi i n f PI3K–AKT–I ignifican l dec ea ed li id d le , dec ea e l de c ibe h ea men -ind ced a c ea men a egie e ide hi i

[, : autophagy; cancer; metabolism;

Supplemental material is available for this a

Received July 25, 2017; revised version accepted October 26, 2017.

Despite significant advances in precision cancer therapies, tumor regressions are variable and rarely complete. Although the molecular basis of how cancer cells survive

maintain bioenergetics (Galluzzi et al. 2015). Additionally, due to the central role that the PI3K–AKT–mTOR pathway has in regulating cellular growth, we reasoned that small molecule inhibitors that converge directly or indirectly on this pathway would similarly induce autophagy to sustain drug-tolerant cells, therefore extending the reach of this mechanism of resistance beyond specific PI3K–AKT–mTOR inhibitors.

Thus far, the therapeutic reflex to block autophagy is to add anti-malarial lysosomotropic inhibitors such as chloroquine, but the clinical responses to these drugs have been variable and noncurative (Goldberg et al. 2012; Shanware et al. 2013; Rosenfeld et al. 2014; Towers and Thorburn 2016). Therefore, it would be clinically impactful to directly target the metabolic enzymes mediating autophagy-fueled metabolic processes on which drug-tolerant cells are dependent. However, there have not been any therapeutically tractable metabolic enzymes identified in the setting of therapy-induced autophagy.

Here, we identify CYT387, a JAK inhibitor that induces autophagy by inhibiting mTOR complex 1 (mTORC1). Consequently, by relieving the inhibitory signal transmitted from mTORC1 to PI3K, treatment with CYT387 leads to activation of the PI3K–mTORC2/AKT pathway. Combining CYT387 with MK2206, an allosteric AKT inhibitor, did not induce any tumor regressions despite effectively inhibiting PI3K–AKT

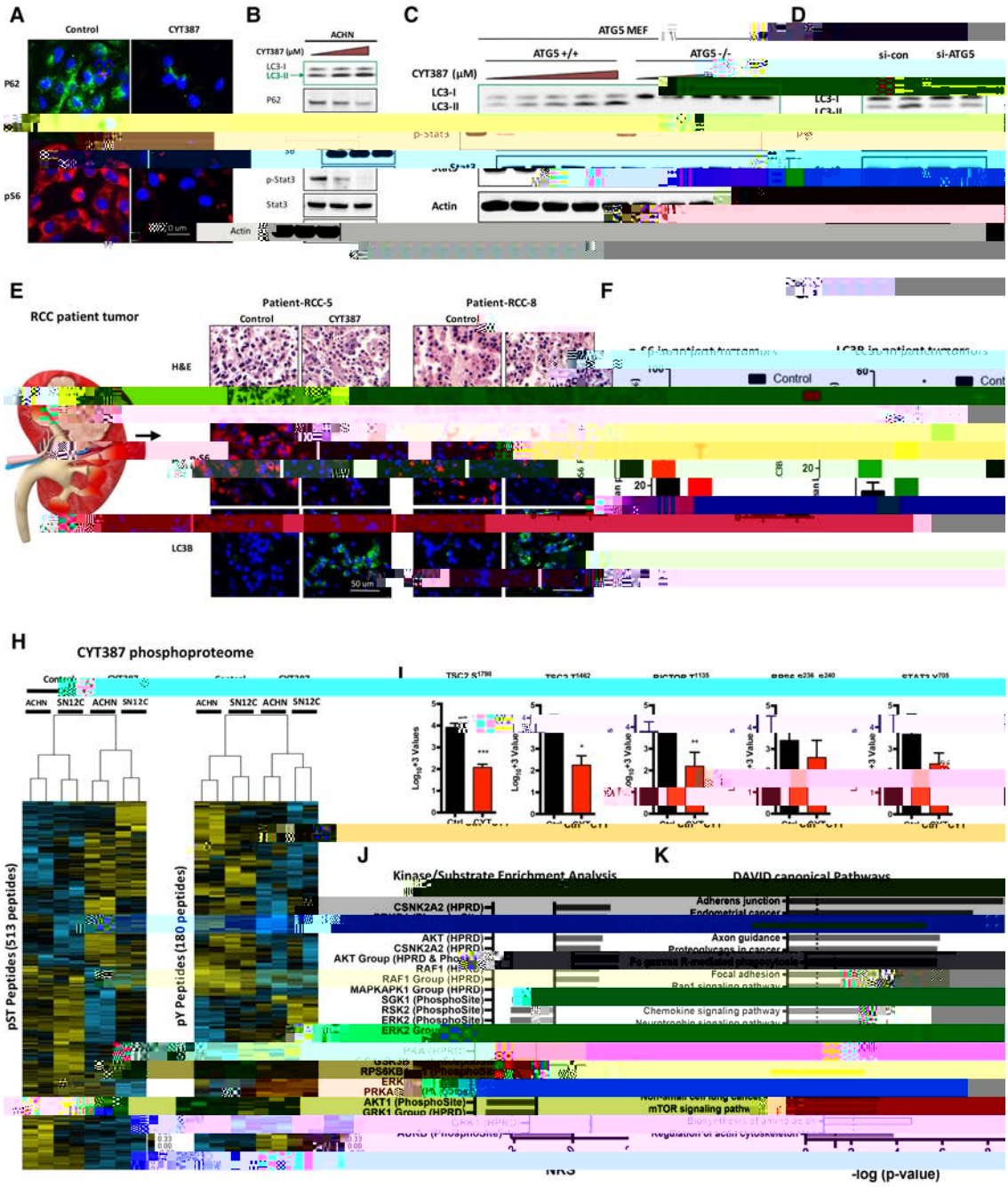

Fig e 1. CYT387 induces autophagy in human cancer cell lines and patient-derived models. ( ) ACHN cells were grown on coverslips, treated with CYT387 for 24 h, and stained p62 and p-S6. ( ) ACHN cells were treated with increasing doses of CYT387 (0–2 μM) and immunoblotted with LC3, p62, p-S6, total S6, p-STAT3, total STAT3, and -actin. ( ) .. $^{+/+}$ and .. $^{-/-}$ MEFs were treated with 0

E64D/pepstatin (which inhibits the protease-induced reconversion of LC3-II into LC3-I), consistent with an increase in autophagosome formation (Supplemental Fig. S2C; Tanida et al. 2005). (4) CYT387 increased the number of double-membraned autophagosomes, which are pathognomonic of autophagy as determined by transmission electron microscopy (Supplemental Fig. S2D; Klionsky et al. 2016). Notably, CYT387 was able to induce autophagy in a dose-dependent manner in murine embryonic fibroblasts (MEFs) that retained the essential autophagy gene ., (., $^{+/+}$), as seen by the lipidation of LC3 (Fig. 1C) (Cecconi and Levine 2008; Fung et al. 2008). Conversely, CYT387 did not induce autophagy in ., -deficient cells (., $^{/}$). Likewise, CYT387-induced autophagy was abrogated with siRNA depletion of ., in ACHN cells (Fig. 1D). To extend our studies into clinical samples, we exposed patient-derived RCC organotypic cultures to CYT387 treatment for 24 h. Importantly, CYT387 significantly induced LCB expression while simultaneously reducing phosphorylated S6 levels (Fig. 1E,F). Taken together, these results indicate that CYT387 treatment induces autophagic flux in both human RCC cell lines and patient-derived tumors.

To obtain further insight into the signaling pathways affected by CYT387 treatment, we studied changes in the phosphoproteome of two different human RCC cells (ACHN and SN12C) after CYT387 treatment using quantitative phosphoproteomics (Rush et al. 2005; Moritz et al. 2010; Zhuang et al. 2013). Supervised hierarchical clustering revealed that 513 phosphoserine and phosphothreonine (pST) peptides and 180 phosphotyrosine (pY) peptides significantly differed between treated and untreated cells (Fig. 1H; Supplemental Tables 2–9). We observed two phosphopeptides to be hypophosphorylated at inhibitory residues T1462 and S1798 in tuberous sclerosis complex 2 (TSC2) in CYT387-treated cells (Manning et al. 2002; Roux et al. 2004). Rapamycin-insensitive companion of mTOR (RICTOR) in CYT387-treated cells was hypophosphorylated at T1135. RICTOR is a subunit of mTORC2 (Kim et al. 2017), but the phosphorylation of T1135 is mediated by mTORC1 via induction of the p70S6 kinase (Julien et al. 2010) and impedes the ability of mTORC2 to phosphorylate AKT on S473 (Fig. 1I; Dibble et al. 2009). As expected, ribosomal protein S6 at residues S236 and S240 and STAT3 Y705 trended toward hypophosphorylation, and p70S6 kinase (RPS6KB) was significantly less active in CYT387-treated cells based on kinase substrate enrichment analyses (KSEAs) (Fig. 1J; Drake et al. 2012). However, KSEAs of AKT motifs were inconclusive, as some motifs trended toward increased activity and others trended toward decreased activity in CYT387-treated cells. DAVID analysis of genes corresponding to the phosphopeptides and activated in CYT387-treated cells (Supplemental Tables 10, 11) also revealed several KEGG (Kyoto Encyclopedia of Genes and Genomes) pathways that are biologically relevant to CYT387 treatment, including glycolysis, amino acid biosynthesis, and central carbon metabolism (Fig. 1K; Huang da et al. 2009a,b). In support of these phosphoproteomics findings, mRNA analysis of CYT387-treated ACHN cells using gene set enrichment analysis (GSEA) of multiple independent data sets revealed significant enrichment of genes involved in several metabolic pathways, while biological modules associated with mTOR (e.g., cell cycle and protein synthesis) were anti-correlated with CYT387 treatment. (Supplemental Tables 12, 13).

Collectively, the phosphoproteome and transcriptome data provide strong evidence that CYT387 treatment reduces mTORC1 signaling to increase TSC2 and mTORC2 signaling leading to AKT activation and is coupled with changes in metabolic pathways.

We reasoned that the CYT387-induced inhibition of mTORC1 would relieve the inhibitory feedback signal normally transmitted from mTORC1 to PI3K, as the phosphoproteomic data suggested via KSEA, and that this would result in hyperactivation of PI3K and AKT, with consequent prosurvival signaling. Consistent with this interpretation, CYT387 treatment caused an increase in AKT T308, the PDK-1-catalyzed site that serves as readout for PI3K signaling in a time-dependent manner (Supplemental Fig. S3A,B). Notably, CYT387 did not dephosphorylate ERK (Supplemental Fig. S3C). Therefore, we sought to identify PI3K–AKT pathway inhibitors that would effectively cooperate with CYT387 to induce apoptosis. We used GDC-0941, a pan-PI3K inhibitor (Sarker et al. 2015); BX795, a PDK-1 inhibitor (Dangelmaier et al. 2014); and MK2206 (Yap et al. 2011), an allosteric AKT inhibitor, to chemically deconstruct this signaling pathway, as depicted in the schematic (Supplemental Fig. S3D–F). We first assessed the biologic effects of these inhibitors on proliferation and apoptosis in human RCC cells singly and in combination with CYT387 (Fig. 2A–D). While GDC-0941, BX795, and MK2206 alone exhibited some anti-proliferative effects, the combination with CYT387 resulted in significantly greater inhibition of proliferation in ACHN and SN12C cells. In marked contrast, all drugs as single agents had little or no effect on apoptosis, but the combination of either agent with CYT387 resulted in increased apoptosis. This was most striking in the CYT387 and MK2206 combination (Fig. 2B,D), and we therefore selected MK2206 for further in vivo studies. We investigated the mechanisms by which MK2206 and CYT387 cooperated to suppress tumor growth in RCC cells (Fig. 2E,F). MK2206 effectively inhibited AKT activation, as documented by dephosphorylation of both p-AKT Thr308 and p-Ser473 and the AKT substrate PRAS40. Consistent with prior results, suppression of AKT induced autophagy, as seen by the conversion of LC3-I to LC3-II. Suppression of mTORC1 by CYT387 led to feedback activation of PI3K, as seen by the increase in phosphorylation of p-AKT Thr308 (which serves as a readout for PI3K activity) and mTORC2 (as monitored by AKT Ser473 phosphorylation). Subsequently, combining MK2206 with CYT387 effectively inhibited both AKT and mTORC1 to almost undetectable levels and induced apoptosis (cleaved caspase 3). Thus, by inhibiting the PI3K–AKT–

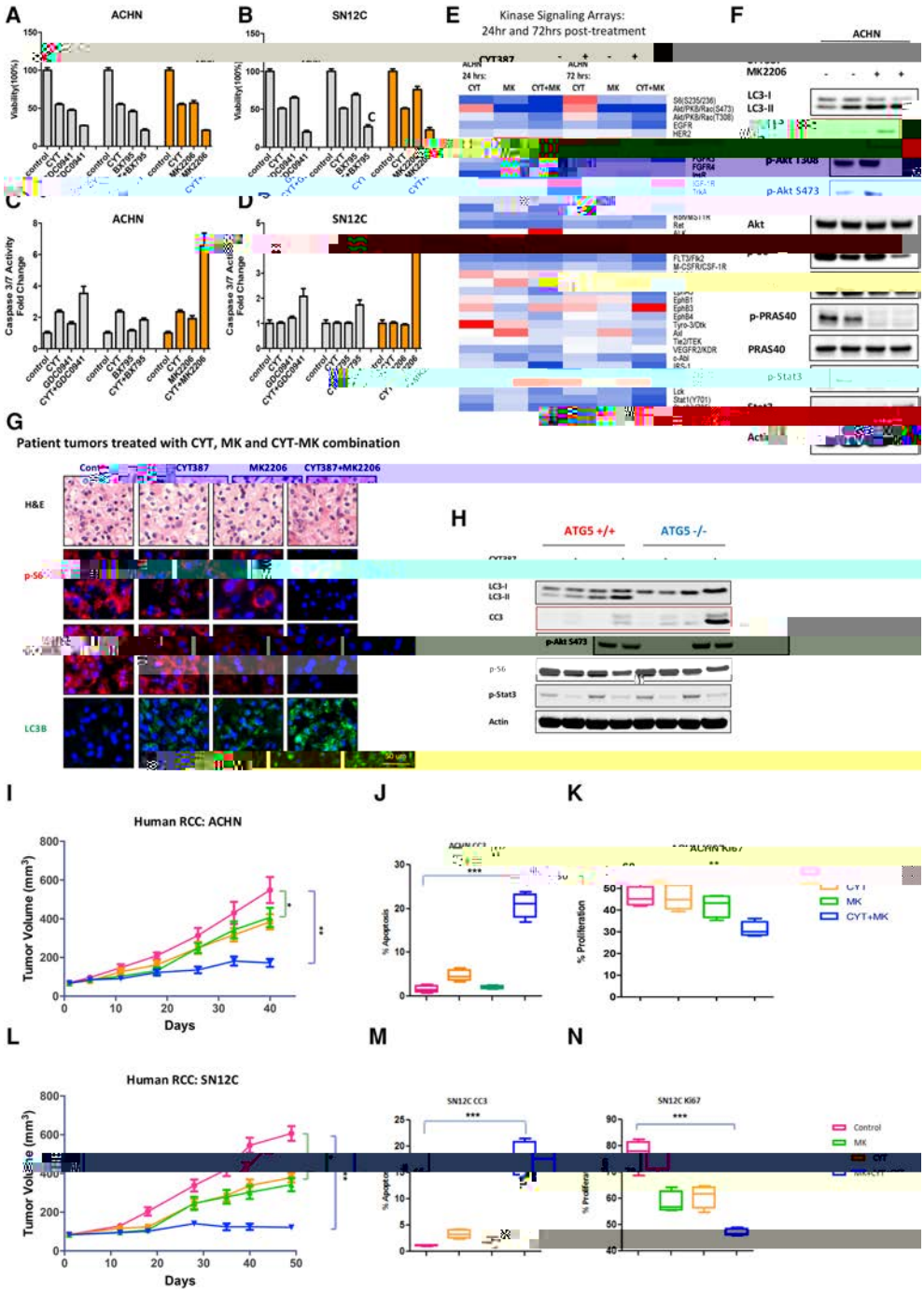

Fig e 2. CYT387 combines with MK2206 to effectively inhibit PI3K–AKT–mTOR signaling in human cancer cell lines and xenografts but does not induce tumor regression. (,) Combination treatment with GDC0941, BX795, and MK2206 with measurement of cell viability in two human RCC cell lines: ACHN ( ) and SN12C ( ). (,) The same combinations as in , with measurement of apoptosis by cleaved caspase 3/7 in ACHN ( ) and SN12C ( ) cells. ( ) A heat map of signaling kinase arrays shows the effects of CYT387, MK2206, and CYT387+MK2206 cotreatment in ACHN cells at 24 h and 72 h after treatment. ( ) Immunoblot for LC3, p-AKT Thr308, p-AKT Ser473, total AKT, p-PRAS40, total PRAS40, p-S6, total S6, p-STAT3, total STAT3, and -actin. ( ) Patient-derived organotypic cultures treated with DMSO (control), CYT387, MK2206, and the CYT387+MK2206 combination for 24 h exhibit an increase in LC3B (green) and a decrease in p-S6 (red) and p-AKT (red). ( ) .. $^{+/+}$ and .. $^{/}$ MEFs were treated with 2 μM CYT387, 10 μM MK2206, and the combination for 24 h, and LC3, cleaved caspase 3, p-AKT, p-S6, p-STAT3, and -actin were evaluated by immunoblotting. ( ) ACHN xenografts treated with vehicle, 50 mg/kg CYT387, 60 mg/kg MK2206, and a 50 mg/kg CYT387 + 60 mg/kg MK2206 combination. Tumor volume is shown. Error bars represent mean ± SEM. Control versus CYT387+MK2206, ( ). < 0.01. (,) The effect on apoptosis (CC3) ( ) and proliferation (KI67) ( ) in ACHN xenograft tumors. Error bars represent mean ± SEM. ( ) Control versus CYT387+MK2206, ( ). < 0.0001. ( ) Control versus CYT387+MK2206, ( ). = 0.0018. (

mTOR pathway at proximal and distal nodes, CYT387 and MK2206 combine to shut down PI3K oncogenic signaling. However, autophagy still persisted in the combination treatment, pointing to a survival signal that sustains subpopulations of drug-tolerant cancer cells. Notably, the CYT387–MK2206 combination induced autophagy in patient-derived organotypic RCC cultures (Fig. 2G).

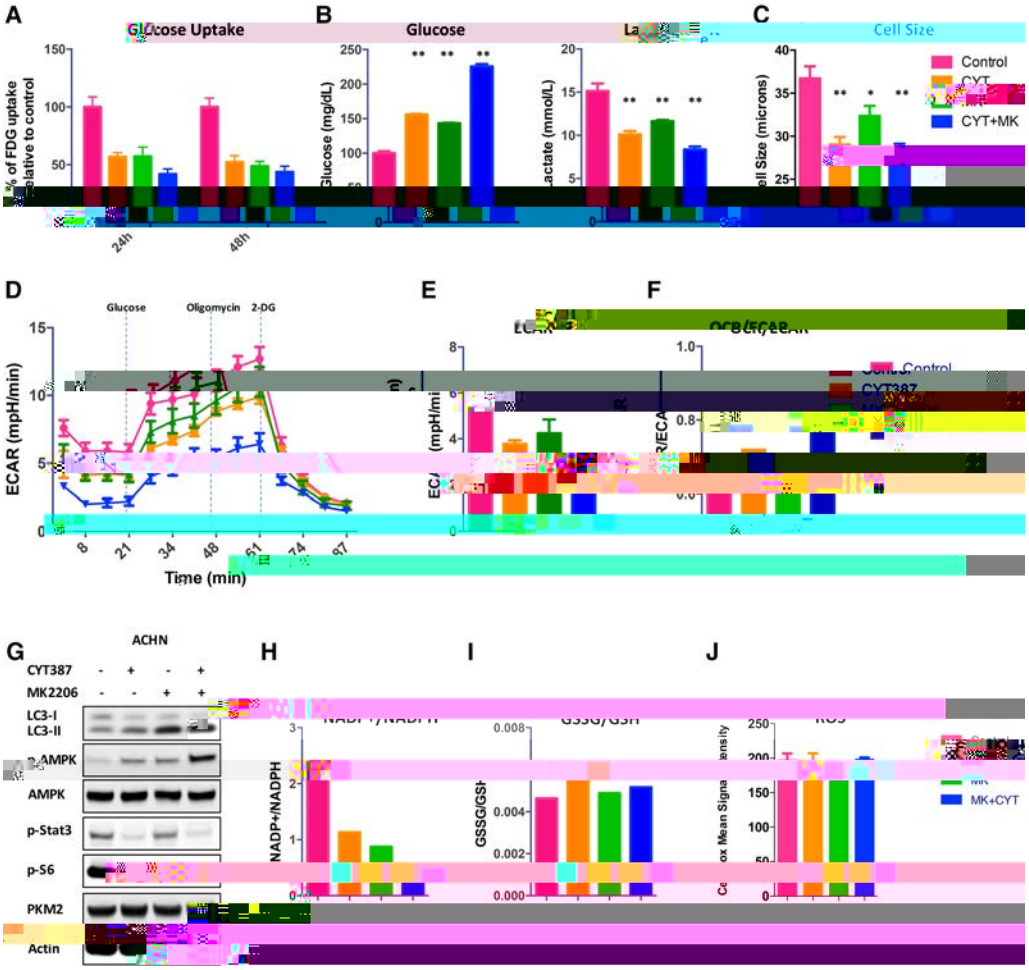

Fig e 3. The effects of treatment on metabolism. ( ) The treatment effects of control, CYT387, MK2206, and CYT387+MK2206 on glucose uptake over time, measured by ^{18}FDG. ( ) Glucose and lactate levels in culture medium were measured in control and treated cells and normalized to cell number. ( ) Qualitative analysis of cell diameter changes of ACHN cells treated with CYT387, MK2206, CYT387 + MK2206, or vehicle (DMSO). ( ) - < 0.02. ( ) Glycolysis in ACHN cells was measured using a XF-96 extracellular flux analyzer after preincubation with drugs or DMSO. Shown are ECAR means ± SD of experimental triplicates. ( ) The effects of treatment on basal ECAR, measured in real time and presented as change in milli-pH per unit time. Representative results are shown. = 2. ( ) Ratios of oxygen consumption rate (OCR; an indicator of OXPHSO) to ECAR (an indicator of aerobic glycolysis at baseline) of treated ACHN cells. Representative results are shown. = 2. (–) Treatment activates p-AMPK and increases NADPH levels, maintains GSSG/GSH ratios, and mitigates reactive oxygen species (ROS). ( ) ACHN cells were treated with control, 2 µM CYT387, 10 µM MK2206, and CYT387 +MK2206 for 24 h and probed with the indicated antibodies. ( ) $NADP^+$/NADPH levels were measured. ( ) GSSG and GSH levels were measured in lysates (= 4) using liquid chromatography-tandem mass spectrometry (LC-MS/MS). ( ) The normalized abundance of these metabolites is shown. Cells were stained with the ROS sensor CellRox. = 3; three independent experiments. - = ns.

consistent with the inhibition of glycolysis (Supplemental Fig. S4A), as described above and also concordant with the gene expression data. Similarly, we also observed reductions in PPP intermediates, amino acids, tricarboxylic acid (TCA) cycle intermediates, and ribose biosynthesis and corresponding increases in purine breakdown products guanine and hypoxanthine (Supplemental Fig. S4B–E). These findings are in keeping with a nutrient-deprived state (i.e., decreased anabolism) with subsequent increased autophagic catabolism to maintain survival (Mizushima et al. 2001). Cells adapt to glucose deprivation by subsisting on fatty acids—mobilized through glycerolipid remodeling—for oxidation, and this is consistent with our observation that the most significant metabolite changes were in lipid intermediates, including phospholipids, triacylglycerol (TAG), cholesterol esters, diacylglycerol (DAG), and fatty acids (C16:0, C18:0, and C18:1) (Fig. 4A; Supplemental Fig. S4F; Kerner and Hoppel 2000; Eaton 2002; Finn and Dice 2006).

We further investigated the lipid substrates that were catabolized by autophagy to produce fatty acids for fatty acid oxidation. Steady-state metabolite profiling showed significant increases in lysophospholipids and arachidonic acid (C20:4), with corresponding decreases in their phospholipid precursors (Fig. 4B). Phospholipids, which include phosphatidylcholine (PC), phosphatidylethanolamine (PE),

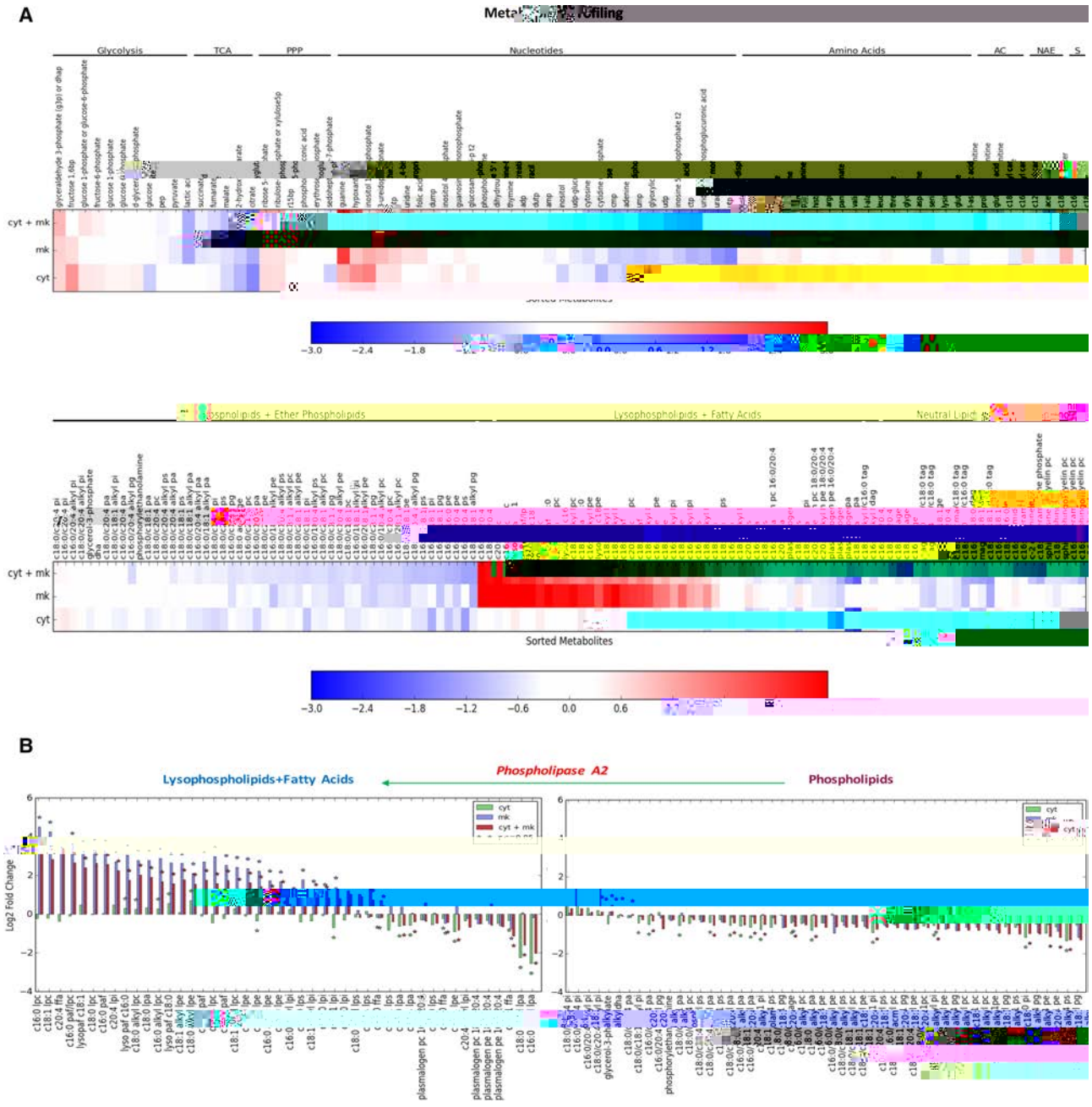

Fig e 4. PI3K–AKT–mTOR signaling inhibition induces metabolic reprogramming. ( ) Heat map of metabolomic profiling of treated cells (CYT387, MKK2206, and CYT387+MMK2206) compared with ACHN cells treated with vehicle (DMSO) using LC-MS/MS (see the Materials and Methods for details). Log fold changes of profiled metabolites are shown. Metabolites are ordered within each category: glycolysis, TCA cycle, PPP, nucleotide metabolism, amino acid metabolism, phospholipids, ether phospholipids, lysophospholipids, fatty acids, neutral lipids, acyl carnithines (AC), sphingolipids (SL), and n-acyl ethanolamines (NACAnes.(5(thats,)-202.-

phosphatidylserine (PS), phosphatidylglycerol (PG), and phosphatidylinositol (PI), are major structural components of cellular membranes. PLA2 is the enzyme that catalyzes the hydrolysis of the phospholipid sn-2 ester bond with subsequent release of lysophospholipids; e.g., lysophosphatidylcholine (LPC), alkly-lysophosphatidylcholine (alkyl-LPC), and free fatty acids (Murakami et al. 2011). Accordingly, we found elevated levels of C16:0 LPC, C18:0 LPC, C18:1 LPC, and C18-0 alkyl-LPC and corresponding decreases in their phospholipid precursors. Notably, we observed significant decreases in free fatty acids (C16:0, C18:0, and C18:1), supporting the idea that

phospholipids are hydrolyzed to supply fatty acids for fatty acid oxidation. Consistent with increased arachidonic acid levels in CYT387–MK2206-cotreated cells, we observed increased levels of 14,15-EET, 11,12-EET, 8,9-EET, and 5-HETE, pointing to arachidonic acid P450-mediated generation of eicosanoids (Supplemental Fig. S5).

To protect cells from the destabilizing effects of excess lipids, free fatty acids mobilized by autophagy and destined for oxidation are stored in an intermediate intracellular pool: LDs (Thiam et al. 2013). We reasoned that the large changes in glycerolipid redistribution identified by our metabolomics profiling of treated cells would result in an increased number of LDs to support fatty acid oxidation, with subsequent mobilization of fatty acids to mitochondria under these nutrient-depleted conditions (Rambold et al. 2015). Consistent with this, we observed that CYT387 and MK2206 singly and in combination incrementally and significantly increased the number and size of Bodipy 493/503-labeled (Fig. 5A–C, green) LDs. Additionally, we incubated ACHN human RCC cells with Bodipy-C12-HPC (a phospholipid containing green fluorescent long chain fatty acid) followed by treatment with vehicle or the CYT387–MK2206 combination. CYT387–MK2206 cotreatment led to a greater degree of incorporation of Bodipy-C12-labeled fatty acids into LDs relative to vehicle-treated cells. This suggests that CYT387–MK2206 treatment-induced autophagy results in phospholipid hydrolysis that releases fatty acids, which are subsequently incorporated into new LDs (Supplemental Fig. S6).

To determine whether the increase in LDs occurred in vivo, we stained the vehicle, CYT387, MK2206, and CYT387–MK2206-cotreated xenograft tumors for adipophilin, which belongs to the perilipin family, members of which coat intracellular lipid storage droplets and facilitate metabolic interactions with mitochondria (Sztalryd and Kimmel 2014). Consistent with the in vitro data, the number of adipophilin-positive LDs significantly and incrementally increased with treatment (as measured on treatment day 40 in ACHN xenograft tumors;

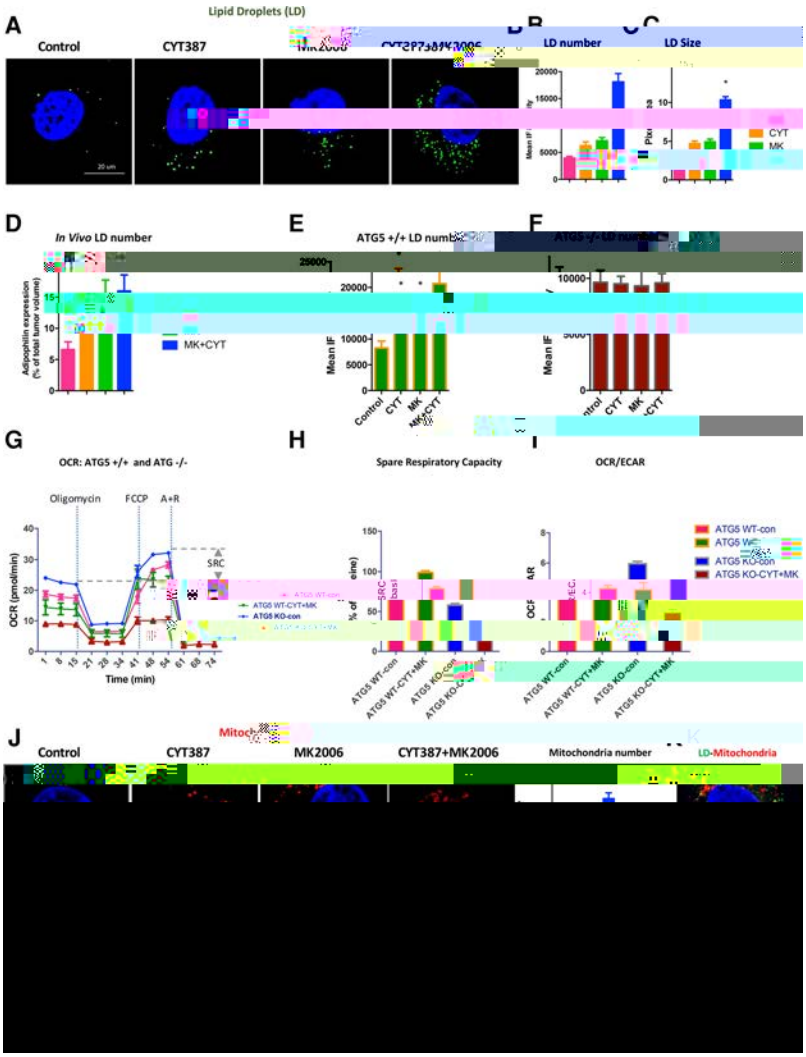

Fig e 5. Autophagy is required for LD growth and fatty acid oxidation. ( ) ACHN cells were treated with control, CYT387, MK2206, and CYT387+MK2206 for 24 h, and Bodipy 493/503 (green) was added to visualize LDs. Representative images are shown. =5 experiments. (,) Bar graphs quantify the increase in number ( ) and size ( ) of LDs, respectively. Data are expressed as means ± SEM. ( ) , <0.001 for control versus n)0.206.3u7.2(052.8(5u7.257.999900e01Tf0.87208463.2811e)17.3(equ

and fatty acids for fatty acid oxidation in treated RCC cells, and, therefore, inhibition of this enzymatic activity would negatively impact OXPHOS and subsequently limit the survival of these cells. To test this directly, we added the PLA2 inhibitor oleyloxyethylphosphocholine (OOEPC; which inhibits secretory PLA) (Slatter et al. 2016) to CYT387, MK2206, and CYT387–MK2206-cotreated cells and measured LD numbers. Addition of OOEPC significantly reduced the LD abundance in CYT387, MK2206, and CYT387–MK2206-cotreated cells

(Fig. 6A,B). Since several isoforms of PLA2 exist, we deter-

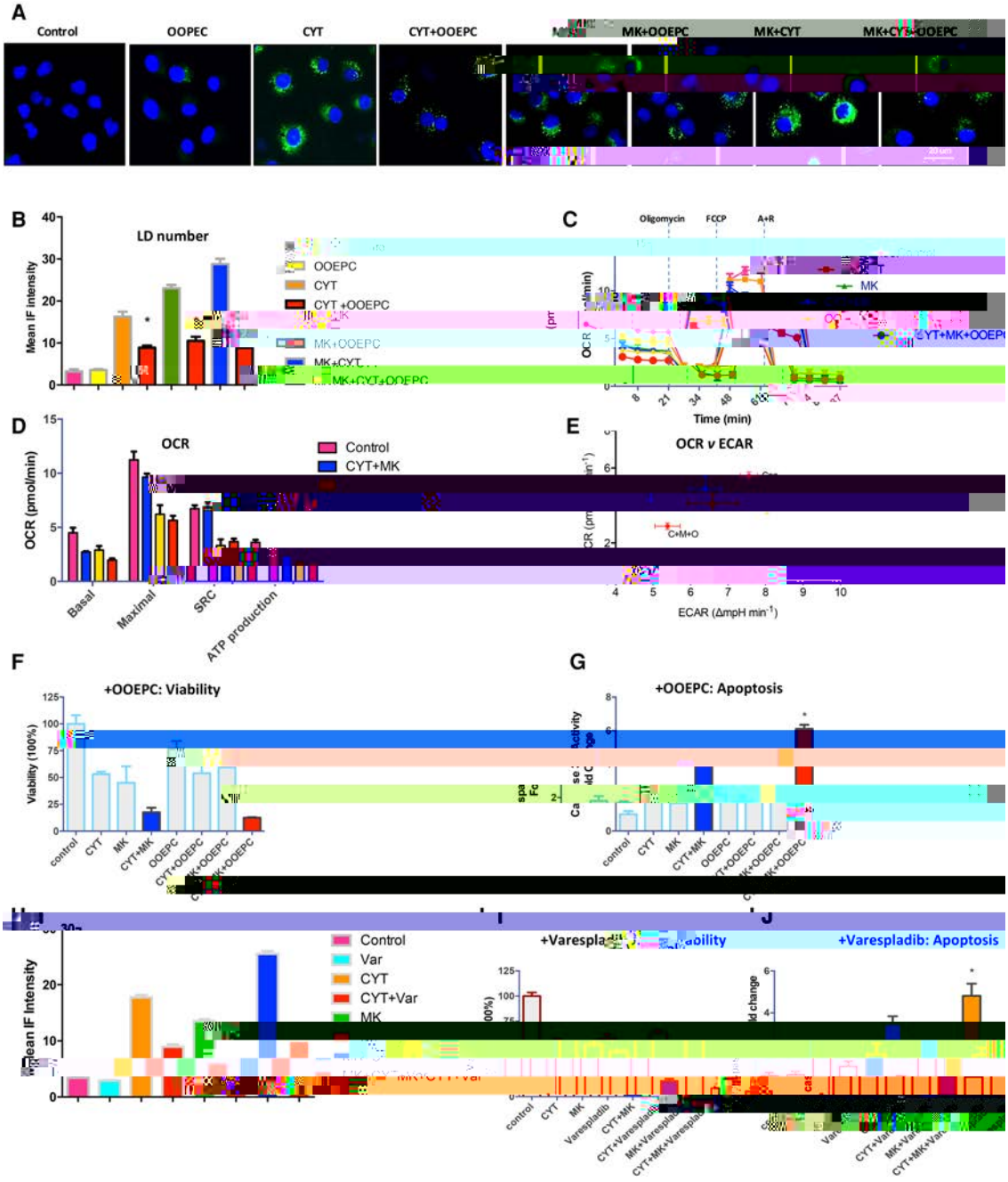

Fig e 6. Hydrolysis of phospholipid supplies lysophospholipids and fatty acids for cancer cell survival. ( ) ACHN cells were treated with

Undoubtedly, the combination of attenuated proliferation signals, nutrient depletion, and metabolic competition for remaining nutrients kills many cells. Accordingly, our data demonstrate that glucose, which is tightly regulated by the PI3K–AKT–mTOR pathway at multiple steps, became limiting with treatment, with a resultant decrease in glycolysis (Engelman et al. 2006; Yecies and Manning 2011; Hu et al. 2016). However, the very same conditions that give rise to these nutrient-deprived microenvironments also induced autophagy. Consequently, the autophagic catabolism of membrane phospholipids provides a ready source of free fatty acids that maintains respiration in subpopulations of cancer cells, therefore enabling their survival in a low-glucose environment. The increase in fatty acid oxidation and OXPHOS requires redox homeostasis, and this is provided by the concomitant activation of AMPK, which increases NADPH, with a subsequent mitigation of ROS. Collectively, treatment-enforced metabolic reprogramming supports cancer cell fitness by providing fatty acids and NADPH to maximize survival.

Since the rate of autophagic release of fatty acids does not match the rate of mitochondrial consumption, these LDs serve a dual purpose: first, as a buffer to reduce lipotoxicity by storing lipid intermediates and, second, to transport these lipids to the mitochondria (Singh et al. 2009; Unger et al. 2010; Rambold et al. 2015). Consequently, these energy-strapped residual cancer cells increase fatty acid oxidation, as it is the most energetically efficient way to generate ATP. Long-lived cell types such as cardiac myocytes and memory T cells (Pearce et al. 2009; Chung et al. 2010) depend on fatty acid metabolism for survival, and we see this as yet another example of cancer cells hijacking normal physiological processes to their benefit.

Our screen identified several structurally different Janus family kinase inhibitors that inhibited mTORC1 and induced autophagic flux. While serendipitous, these findings are not unexpected, as small molecules inhibit several kinases and would directly and/or indirectly interdict the PI3K–AKT–mTOR pathway. To date, JAK inhibitors have been approved for and/or are undergoing late stage clinical trials in MPN, including the focus of this study, CYT387 (momelutinib) (Patel et al. 2016; Winton and Kota 2017). However, complete cytogenetic or molecular responses with JAK inhibitors have not been observed, with clinical benefit mainly resulting from improved performance status due to reduced cytokine levels rather than the elimination of cancer cells (Verstovsek

A seven-point dilution series of 116 small molecule inhibitors covering a 1000× concentration range was plated into three 384-well plates using the EP Motion automated dispensing system. Control wells with equal volumes of DMSO were included as negative controls. ACHN cells were grown, trypsinized, counted, and plated directly into warm drug plates using a Multidrop

manufacturer's protocol, with 150 µg of protein being used for each experiment. Signal intensity was calculated using a LI-COR Odyssey imaging system, and fluorescent intensity was quantified using the Odyssey software where indicated.

^{18}F-FDG uptake

^{18}F-FDG was purchased from the radiopharmacy at University of California at San Francisco. SN12C or ACHN cells (5×10^5 cells) were plated and exposed to vehicle or drug for 24 and 48 h, whereupon the cells were incubated with 0.5 Ci of ^{18}F-FDG for 1 h at 37°C. The ^{18}F-FDG in the medium and the intracellular ^{18}F-FDG were isolated and counted using a counter. The intracellular ^{18}F-FDG was expressed as a percentage of the total activity added to cells normalized to the cell number.

Metabolomics

Metabolomic data and single-reaction monitoring (SRM) transitions were performed as described previously (Camarda et al. 2016) and are in Supplemental Table 13. Briefly, 2 million cells were plated overnight and serum-starved for 2 h prior to harvesting, after which cells were washed twice with PBS, harvested by scraping, and flash-frozen. For nonpolar metabolomic analyses, flash-frozen cell pellets were extracted in 4 mL of 2:1:1 chloroform/methanol/PBS with internal standards: 10 nmol of dodecylglycerol and 10 nmol of pentadecanoic acid. Organic and aqueous layers were separated by centrifugation, and the organic layer was extracted. The aqueous layer was acidified with 0.1% formic acid followed by re-extraction with 2 mL of chloroform. The second organic layer was combined with the first extract and dried under nitrogen, after which lipids were resuspended in 120 µL of chloroform. A 10-µL aliquot was then analyzed by both SRM-based LC-MS/MS or untargeted LC-MS. For polar metabolomic analyses, frozen cell pellets were extracted in 180 µL of 40:40:20

Drake JM, Graham NA, Stoyanova T, Sedghi A, Goldstein AS, Cai H, Smith DA, Zhang H, Komisopoulou E, Huang J, et al. 2012. Oncogene-specific activation of tyrosine kinase networks during prostate cancer progression. **109:** 1643–1648.

Drake JM, Paull EO, Graham NA, Lee JK, Smith BA, Titz B, Stoyanova T, Faltermeier CM, Uzunangelov V, Carlin DE, et al. 2016. Phosphoproteome integration reveals patient-specific networks in prostate cancer. **166:** 1041–1054.

Duvel K, Yecies JL, Menon S, Raman P, Lipovsky AI, Souza AL, Triantafellow E, Ma Q, Gorski R, Cleaver S, et al. 2010. Activation of a metabolic gene regulatory network downstream of mTOR complex 1. **39:** 171–183.

Eaton S. 2002. Control of mitochondrial -oxidation flux. **41:** 197–239.

Eisen MB, Spellman PT, Brown PO, Botstein D. 1998. Cluster analysis and display of genome-wide expression patterns. **95:** 14863–14868.

Engelman JA, Luo J, Cantley LC. 2006. The evolution of phosphatidylinositol 3-kinases as regulators of growth and metabolism. **7:** 606–619.

Finn PF, Dice JF. 2006. Proteolytic and lipolytic responses to starvation. **22:** 830–844.

Fruman DA, Rommel C. 2014. PI3K and cancer: lessons, challenges and opportunities. **13:** 140–156.

Fung C, Lock R, Gao S, Salas E, Debnath J. 2008. Induction of 11T830-7570Tang-Goldber-

cane[illegible]

Rebecca VW, Amaravadi RK. 2016. Emerging strategies to effectively target autophagy in cancer. **35:** 1–11.

Rosenfeld MR, Ye X, Supko JG, Desideri S, Grossman SA, Brem S, Mikkelson T, Wang D, Chang YC, Hu J, et al. 2014. A phase I/II trial of hydroxychloroquine in conjunction with radiation therapy and concurrent and adjuvant temozolomide in patients with newly diagnosed glioblastoma multiforme. **10:** 1359–1368.

Rosenson RS, Hislop C, Elliott M, Stasiv Y, Goulder M, Waters D. 2010. Effects of varespladib methyl on biomarkers and major cardiovascular events in acute coronary syndrome patients. **56:** 1079–1088.

Roux PP, Ballif BA, Anjum R, Gygi SP, Blenis J. 2004. Tumor-promoting phorbol esters and activated Ras inactivate the tuberous sclerosis tumor suppressor complex via p90 ribosomal S6 kinase. **101:** 13489–13494.

Rush J, Moritz A, Lee KA, Guo A, Goss VL, Spek EJ, Zhang H, Zha XM, Polakiewicz RD, Comb MJ. 2005. Immunoaffinity profiling of tyrosine phosphorylation in cancer cells. **23:** 94–101.

Saldanha AJ. 2004. Java Treeview—extensible visualization of microarray data. **20:** 3246–3248.

Sarker D, Ang JE, Baird R, Kristeleit R, Shah K, Moreno V, Clarke PA, Raynaud FI, Levy G, Ware JA, et al. 2015. First-in-human phase I study of pictilisib (GDC-0941), a potent pan-class I phosphatidylinositol-3-kinase (PI3K) inhibitor, in patients with advanced solid tumors. **21:** 77–86.

Sehgal AR, Konig H, Johnson DE, Tang D, Amaravadi RK, Boyiadzis M, Lotze MT. 2015. You eat what you are: autophagy inhibition as a therapeutic strategy in leukemia. **29:** 517–525.

Shanware NP, Bray K, Abraham RT. 2013. The PI3K, metabolic, autophagy networks: interactive partners in cellular health and disease. **53:** 89–106.

Singh R, Kaushik S, Wang Y, Xiang Y, Novak I, Komatsu M, Tanaka K, Cuervo AM, Czaja MJ. 2009. Autophagy regulates lipid metabolism. **458:** 1131–1135.

Slatter DA, Aldrovandi M, O'Connor A, Allen SM, Brasher CJ, Murphy RC, Mecklemann S, Ravi t501rS,O

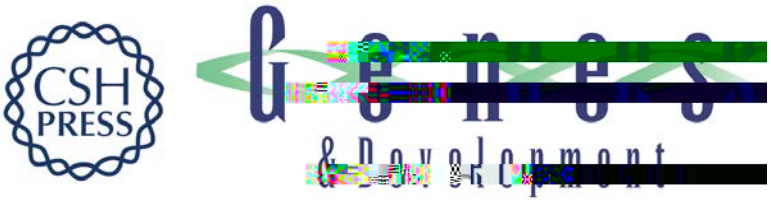

Metabolic reprogramming ensures cancer cell survival despite oncogenic signaling blockade

Hui-wen Lue, Jennifer Podolak, Kevin Kolahi, et al.

Genes Dev. 2017, 31: originally published online November 14, 2017
Access the most recent version at doi:10.1101/gad.305292.117